Lateral patterning of multilayer InAs/GaAs(001) quantum dot structures by *in vacuo* focused ion beam

2012 Nanotechnology 23 135401

(http://iopscience.iop.org/0957-4484/23/13/135401)

Nanotechnology **23** (2012) 135401 (7pp) doi:10.1088/0957-4484/23/13/135401

Lateral patterning of multilayer InAs/GaAs(001) quantum dot structures by *in vacuo* focused ion beam

A J Martin[1], T W Saucer[2], G V Rodriguez[2], V Sih[2] and J M Millunchick[1,3]

[1] Department of Materials Science and Engineering, University of Michigan, Ann Arbor, MI 48109, USA
[2] Department of Physics, University of Michigan, Ann Arbor, MI 48109, USA

E-mail: joannamm@umich.edu

Received 21 December 2011, in final form 24 February 2012
Published 16 March 2012
Online at stacks.iop.org/Nano/23/135401

Abstract
We report on the effects of patterning and layering on multilayer InAs/GaAs(001) quantum dot structures laterally ordered using an *in vacuo* focused ion beam. The patterned hole size and lateral pattern spacing affected the quantum dot size and the fidelity of the quantum dots with respect to the lateral patterns. 100% pattern fidelity was retained after six layers of dots for a 9.0 ms focused ion beam dwell time and 2.0 μm lateral pattern spacing. Analysis of the change in quantum dot size as a function of pattern spacing provided a means of estimating the maximum average adatom surface diffusion length to be approximately 500 nm, and demonstrated the ability to alter the wetting layer thickness via pattern spacing. Increasing the number of layers from six to 26 resulted in mound formation, which destroyed the pattern fidelity at close pattern spacings and led to a bimodal quantum dot size distribution as measured by atomic force microscopy. The bimodal size distribution also affected the optical properties of the dots, causing a split quantum dot photoluminescence peak where the separation between the split peaks increased with increasing pattern spacing.

(Some figures may appear in colour only in the online journal)

1. Introduction

Quantum dots (QD) are of interest for applications such as intermediate band solar cells [1, 2], lasers [3, 4], and quantum computing. For these applications, it is advantageous to control the QD dimensions and areal density because these properties directly influence the optical and electronic properties of QD structures. Additionally, control of the QD position is beneficial for some quantum computing technologies where coupling of QDs to photonic crystal cavities requires precise QD positioning to achieve good spatial and spectral overlap of the QD and cavity mode [5, 6]. InAs QDs are typically grown by self-assembly via the Stranski–Krastanov growth mode. When using this growth mode, the QD position is random and the size is primarily controlled by the growth temperature, deposition rate, and the amount of material deposited. Preferential QD nucleation can be achieved by altering the surface morphology in specific areas, providing a means of controlling the dot placement. InAs/GaAs QDs have been shown to preferentially nucleate on focused ion beam (FIB) irradiated surfaces prior to reaching the critical thickness for nucleation on non-irradiated surfaces [7]. Furthermore, lateral ordering of QDs has been demonstrated on pre-patterned arrays of holes via methods such as *ex vacuo* e-beam lithography [8, 9] and *in vacuo* FIB patterning for Ge/Si QDs [10–12] and InAs/GaAs QDs [13–16]. Macro- and micro-photoluminescence have been measured from lithographically patterned [17] and FIB-patterned [15, 19] InAs/GaAs QDs. Additionally, single

[3] Address for correspondence: 2300 Hayward Street, Ann Arbor, MI 48109, USA.

QD emission with a line width of 160 μeV has been measured from FIB-patterned QDs [14].

Directed growth techniques are valuable because lateral patterning provides better control over QD density and position [14, 18, 19]. *Ex vacuo* patterning techniques require exposure to air between patterning and QD growth, resulting in the formation of an oxide layer, which must be removed prior to QD growth and can negatively affect the optical properties of the dots [20]. In contrast, *in vacuo* FIB patterning can be used to produce laterally ordered QDs while keeping the sample within the protective confines of the vacuum at all times. Previous work has demonstrated the effects of FIB patterning conditions on single layers of QDs [13, 15, 16] and on the optical properties of multilayer FIB-patterned QD structures [15, 19]. In this work, we demonstrate the effects of *in vacuo* FIB patterning on the QD diameter, density, pattern fidelity, and optical properties as well as the effect of increased layering on the surface morphology for multilayer InAs/GaAs QD structures. We also demonstrate FIB patterning as a method for estimating the maximum adatom diffusion length for a given set of growth conditions and as a means of altering the wetting layer thickness.

2. Experimental procedure

Two multilayer InAs/GaAs(001) QD structures were grown by molecular beam epitaxy (MBE) on FIB-patterned GaAs(001) substrates. Figure 1 is a schematic of the multilayer structures grown. A 500 nm GaAs buffer layer was grown on both samples at $T = 590\,^{\circ}$C. Following buffer growth, the samples were transferred *in vacuo* to the focused ion beam (FIB) for patterning of 40×40 μm^2 arrays of holes. The holes were FIB-milled with a single pass of a 10 pA, 30 keV Ga^+ focused ion beam. The FIB dwell times were 1.0, 3.0, 6.0, and 9.0 ms, each at pattern spacings of 0.25, 0.5, 1.0, and 2.0 μm, for a total of 16 different patterns. The FIB dwell time determined the dimensions of the FIB-milled holes. After patterning, the samples were transferred *in vacuo* back to the MBE for QD growth. 2.0 monolayers (ML) of InAs was deposited at $T = 485\,^{\circ}$C for the QDs at a rate of 0.11 ML s^{-1} and immediately capped with GaAs at a rate of 1.0 ML s^{-1}. The QD growth and GaAs capping process was repeated, creating multilayer structures with six and 26 layers. The spacer layer thickness was 20 nm for the six layer sample and 18 nm for the 26 layer sample. The topmost layer of QDs remained uncapped for both samples for analysis by atomic force microscopy (AFM).

3. Data analysis

For the six layer sample, the QDs on the uncapped surface nucleated only in the patterned areas and only above the patterned sites due to the formation of preferential nucleation sites created at the initial layer by the FIB [7, 13, 14, 19]. The holes were milled only at the substrate for both samples (see figure 1). The dimensions of the FIB-milled holes were measured on a separate sample. The hole dimensions increased linearly in size from 85 ± 9 nm in diameter and 3.0 ± 0.3 nm in depth for a 1.0 ms FIB dwell time to 133 ± 14 nm in diameter and 12 ± 1 nm in depth for a 9.0 ms FIB dwell time. Figures 2(a) and (b) show plots of the hole dimensions as a function of FIB dwell time for a 2.0 μm pattern spacing. Figure 3 shows AFM images of the uncapped sixth layer for the 1.0, 3.0, 6.0, and 9.0 ms FIB dwell time patterns each at a pattern spacing of 2.0 μm. The QDs at the sixth layer were aligned above the underlying FIB-milled holes. All areas away from the holes were devoid of QDs because the deposited InAs thickness was below the critical thickness for QD nucleation on a planar surface for the given growth conditions. Figures 2(a) and (b) also show plots of the QD dimensions at the sixth layer as a function of FIB dwell time for a 2.0 μm pattern spacing. All QD measurements were performed by a watershed technique, which employed a slope per cent to determine a baseline for measuring QD diameter and height. The QDs increased in size with increasing FIB dwell time from 47 ± 12 nm in diameter and 5 ± 2 nm in height for the 1.0 ms FIB dwell time to 91±28 nm in diameter and 15 ± 8 nm in height for the 9.0 ms FIB dwell time. The difference in size between the QDs on the longer and shorter FIB dwell time patterns may be due to a tendency for multi-dot nucleation on the shorter two FIB dwell time patterns (figure 2(c) and inset in figure 3(a)). For the 1.0 and 3.0 ms FIB dwell time patterns, the FIB-milled holes at the substrate were smaller and shallower, and thus more likely to fill during GaAs capping and layering than the larger, deeper holes milled by the 6.0 and 9.0 ms FIB dwell times. Complete or partial filling of the smaller holes resulted in a smoother surface where either no QDs formed or multiple dots formed at a single patterned site due to the step edge density at those locations. In contrast, the steep sidewalls of the partially filled holes milled by the longer FIB dwell times forced the InAs down toward the bottom of the holes, forming a single QD as shown in the inset in figure 3(d). Kinetic Monte Carlo simulations by Lee *et al* demonstrate these same principles for InAs QD formation on FIB-patterned GaAs, resulting in QD nucleation at the bottom of the FIB-milled holes when the sidewalls are steep [13].

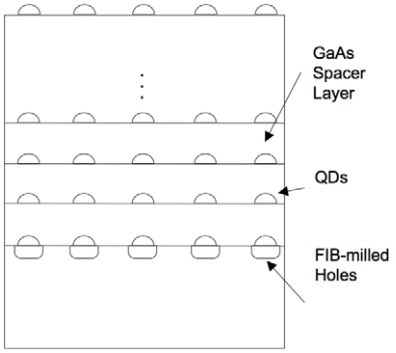

Figure 1. A schematic of the FIB-patterned six and 26 layer InAs/GaAs QD structures. Square arrays of FIB-milled holes were patterned at the substrate with pattern spacings of 0.25, 0.5, 1.0, and 2.0 μm each at FIB dwell times of 1.0, 3.0, 6.0, and 9.0 ms. 2.0 ML of InAs was deposited for the QDs for both samples. The GaAs spacer layer thicknesses were 20 and 18 nm for the six and 26 layer samples, respectively.

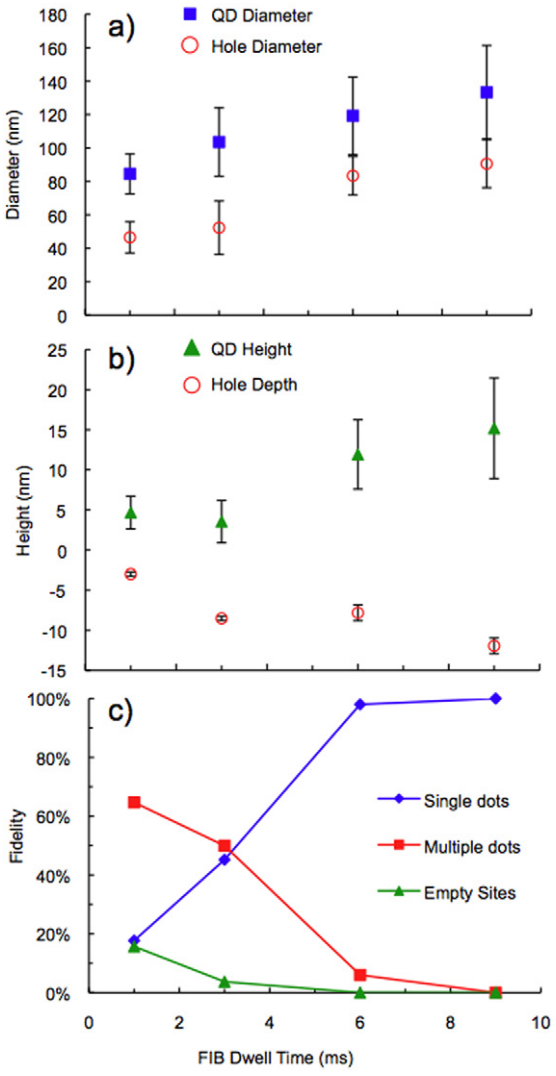

Figure 2. Plots of (a) QD diameter as measured at the sixth layer and FIB-milled hole diameter as measured at the substrate of a separate sample; (b) QD height as measured at the sixth layer and FIB-milled hole depth as measured at the substrate of a separate sample; (c) pattern fidelity as a function of FIB dwell time. All data are for the 2.0 μm pattern spacing as measured on the uncapped surface of the six layer sample.

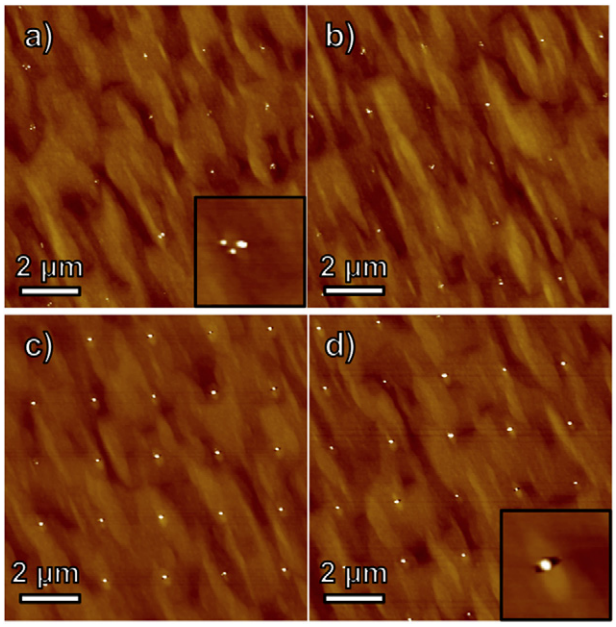

Figure 3. AFM images of the uncapped surface of the six layer sample for the 2.0 μm spacing patterns at FIB dwell times of (a) 1.0 ms, (b) 3.0 ms, (c) 6.0 ms, and (d) 9.0 ms. The inset in (a) shows a higher magnification image of the multi-dot nucleation and the inset in (d) shows the concave shape of the FIB pattern, which did not completely planarize upon layering for the 6.0 and 9.0 ms dwell times.

For all FIB dwell times, the original pattern was retained with some level of fidelity despite the relatively thick GaAs spacer layer. This demonstrates that FIB patterning can extend the maximum spacer layer thickness achievable for retaining vertical alignment of QDs, which Xie *et al* found to be approximately 7 nm for 90–100% strain correlation between layers of unpatterned InAs/GaAs QDs grown with the same InAs deposited thickness we report and at a growth temperature 15 °C hotter [21, 22]. Some researchers have reported vertical QD alignment for spacer layers as thick as 30 nm when the amount of InAs deposited for dot formation was thicker and/or the growth temperature was higher [23, 24] than reported here. In this work, the critical thickness for QD nucleation on a planar surface has not been surpassed. Therefore, the vertical QD alignment is not likely to be solely a result of island-induced strain. Instead, it is likely due to the relatively large size of our FIB-induced QDs, which were 5–15 nm in height, coupled with any additional strain in the substrate due to FIB patterning. For the longer FIB dwell times, pattern retention may also be due to the concave shape of only partially filled, non-planarized holes, which persisted through to the sixth layer. To further analyze the effects of hole filling on layer-to-layer pattern retention, the fidelities of single and multi-dot formation per patterned site as well as the percentage of empty sites were measured. Figure 2(c) shows the single QD, multi-dot, and empty site fidelities with increasing FIB dwell time for the 2.0 μm pattern spacings. Single QD fidelity increased from only 18% for the 1.0 ms FIB dwell time to nearly 100% for both the 6.0 and 9.0 ms FIB dwell time patterns. The fraction of multi-dot nucleation and empty sites decreased with increasing FIB dwell time, which was likely due to hole filling as previously discussed.

The pattern spacing was varied from 0.25 to 2.0 μm to analyze its effect on QD size and pattern fidelity. Figures 4(a)–(d) show AFM images of the uncapped sixth layer for the 0.25, 0.5, 1.0, and 2.0 μm pattern spacings at a 9.0 ms FIB dwell time. Varying the pattern spacing did not significantly affect the fidelity of single QDs. However, QD size increased with increasing pattern spacing with the diameter saturating at approximately 90 nm for the 9.0 ms FIB dwell time patterns as shown in the plot in figure 4(e). This effect can be explained in terms of the adatom surface diffusion length, which determines the capture zone of the FIB-milled hole [25, 26]. For unpatterned surfaces, QD position, size, and areal density are limited in part by the capture zone, which is generally determined by the growth conditions (e.g.,

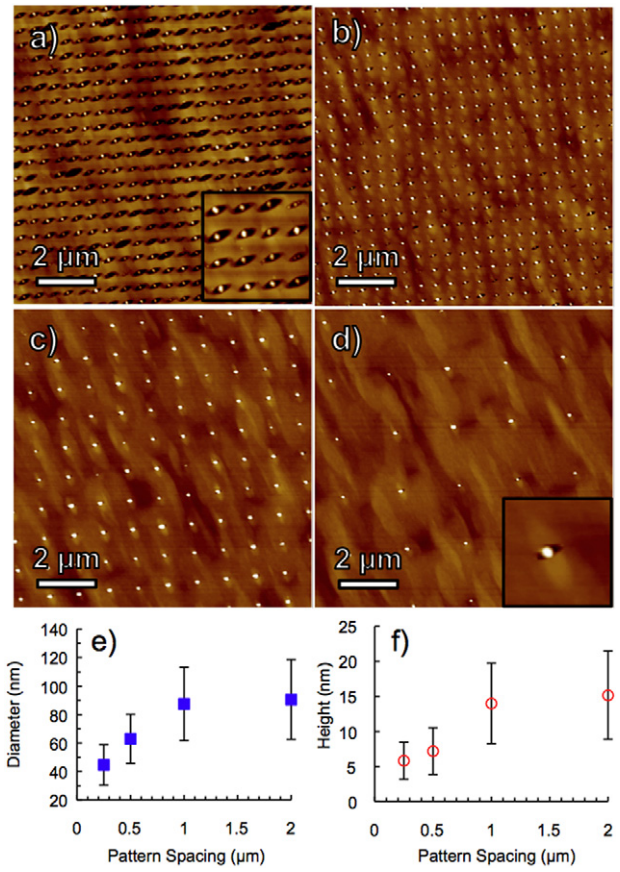

Figure 4. AFM images of the uncapped surface of the six layer sample for the 9.0 ms FIB dwell time patterns at pattern spacings of (a) 0.5 μm, (b) 0.5 μm, (c) 1.0 μm and (d) 2.0 μm. The insets in (a) and (d) show higher magnification images of the QDs. The concave shape of the holes (small, dark area beside the QDs) is shown to persist through to the sixth layer. (e), (f) Plots of the QD diameter and height as a function of pattern spacing for the 9.0 ms FIB dwell time patterns of the six layer sample.

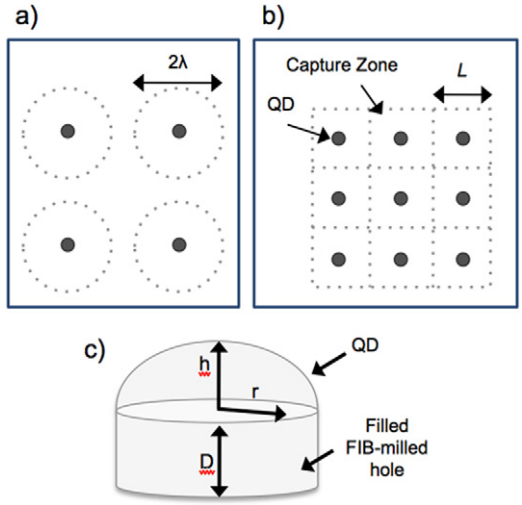

Figure 5. Schematics showing the change in the capture zone for (a) close pattern spacings and (b) larger pattern spacings. (c) A schematic of the ellipsoid and cylinder shapes used to approximate the QD volume for the wetting layer thickness estimation.

temperature and growth rate) [26]. However, by creating preferential nucleation sites using the FIB and reducing the thickness of the deposited InAs to below the critical thickness for dot nucleation on a planar surface, QD position and size can instead be controlled by the capture zone of the patterned hole and not the QD. Figures 5(a) and (b) illustrate how the capture zone of the patterned holes changes for large and small pattern spacings. If the pattern spacing is large enough, adatoms moving along the surface can only reach either one or zero FIB-milled holes before coming to rest. Therefore, the adatom diffusion length limits the capture zone of the patterned hole. The volume of InAs available per patterned site, V_{InAs}, for QD nucleation is then determined by the maximum adatom diffusion length, λ, for the given growth conditions and the deposited InAs thickness, t, as

$$V_{\mathrm{InAs}} = t\pi\lambda^2. \tag{1}$$

Therefore, increasing the pattern spacing beyond this distance will not result in a change in QD size without altering the growth conditions (e.g., changing the growth temperature or the deposited InAs thickness). However, as the pattern spacing decreases to less than the maximum adatom diffusion length, the capture zones of neighboring patterned holes begin to overlap and V_{InAs} is no longer dependent on the maximum diffusion length, but on the pattern spacing, L, as

$$V_{\mathrm{InAs}} = tL^2. \tag{2}$$

The measured QD diameter and height are consistent with this analysis, showing a decrease in size once the pattern spacing decreases below approximately 1.0 μm (figure 4(e)), which is equivalent to a maximum average adatom diffusion length of approximately 500 nm for the given growth conditions.

The diffusion length at each pattern spacing can be used in conjunction with the measured QD dimensions to estimate the thickness of the WL as a function of the pattern spacing. The minimum thickness of the WL was estimated for the 9.0 ms FIB dwell time patterns at each pattern spacing. The volume of the QD was estimated as half of an ellipsoid (see figure 5(c)) with an additional volume added to take into account InAs filling of the FIB-milled holes, which were not planarized at the sixth layer for the 9 ms FIB dwell time patterns (see insets in figure 4). This additional QD volume was estimated as a cylinder (see figure 5(c)) with height, D, equal to the maximum depth of the FIB-milled holes as measured at the substrate and radius, r, equal to that of the QDs based on observations from the AFM images (see figure 4) such that

$$V_{\mathrm{QD}} = \tfrac{2}{3}\pi r^2 h + \pi r^2 D. \tag{3}$$

Although the hole dimensions at the sixth layer may be slightly smaller than at the first layer, using the hole dimensions from the first layer provided an overestimation of the QD volume, ensuring a minimum estimate of the WL thickness. The WL thickness, t_{WL}, is estimated by setting the volume of InAs deposited within the capture zone, V_{InAs}, equal to the sum of the WL and QD (equation (3)) volumes

such that

$$V_{\mathrm{InAs}} = (A_{\mathrm{WL}} - \pi r^2)t_{\mathrm{WL}} + V_{\mathrm{QD}} \quad (4)$$

where A_{WL} is the area of the WL and πr^2 is the area of the FIB-patterned hole. For the 1.0 and 2.0 μm pattern spacings, equation (1) is used for V_{InAs} and A_{WL} is assumed to be a circle (figure 5(a)) with a radius of 500 nm in accordance with the estimated maximum average adatom diffusion length. For the 0.5 and 0.25 μm pattern spacings, equation (2) is used for V_{InAs} and A_{WL} is assumed to be a square (figure 5(b)) with side length equal to the pattern spacing. Solving for t_{WL} gives a WL thickness of approximately 1.4 ML for the 1.0 and 2.0 μm pattern spacings, decreasing to 1.3 and 0.7 ML for the 0.5 and 0.25 μm pattern spacings, respectively. The estimated WL thickness follows the same trend with decreasing pattern spacing as the QD diameter and height (figure 4(e)), decreasing at a pattern spacing of approximately 1.0 μm. Some reports have shown changes in QD size and WL thickness upon layering of QDs [23, 27]. However, the changes in QD dimensions and WL thickness described in this work are a function of the pattern spacing only and are, therefore, independent of the layering.

Knowledge of the maximum average adatom diffusion length is advantageous because it provides an ability to tune the QD and WL dimensions. For example, if the pattern spacing is less than the maximum average diffusion length, the QD and WL dimensions can be tailored by altering the pattern spacing. However, if the pattern spacing is greater than the maximum average diffusion length, altering the pattern spacing no longer affects the QD size so the areal density can be changed without affecting the dimensions of the QDs. This ability to tune the QD and WL dimensions by FIB patterning also provides some control over their optical and electronic properties. It is important to note that the adatom diffusion lengths estimated here are for the specific growth and patterning conditions. Therefore, changing these conditions may provide an additional means of adjusting the diffusion length, providing further control over the QD properties.

Increasing the total number of layers of QDs from six to 26 resulted in mound formation above the underlying patterned sites. Figures 6(a)–(d) show AFM images of the uncapped 26th layer for the 0.25, 0.5, 1.0, and 2.0 μm pattern spacings at a 9.0 ms FIB dwell time. At larger pattern spacings, it was evident that mound formation occurred only above the underlying FIB-patterned sites. The mounds were approximately 800–1000 nm in length along $[1\bar{1}0]$, independent of the FIB dwell time or pattern spacing. The mounds on the 9.0 ms FIB dwell time patterns had a length/width aspect ratio of approximately three, whereas the mounds on the other patterns had a length/width ratio of approximately two. Uncapped surface QDs showed a tendency to form on the top and sides of the mounds as shown in the insets in figures 6(c) and (d), which were likely lower energy sites due to an increase in step density. Kiravittaya *et al* reported mounds aligned along $[1\bar{1}0]$ on the uncapped surface of a six layer QD structure patterned by standard optical lithography with a similar spacer thickness (15 nm).

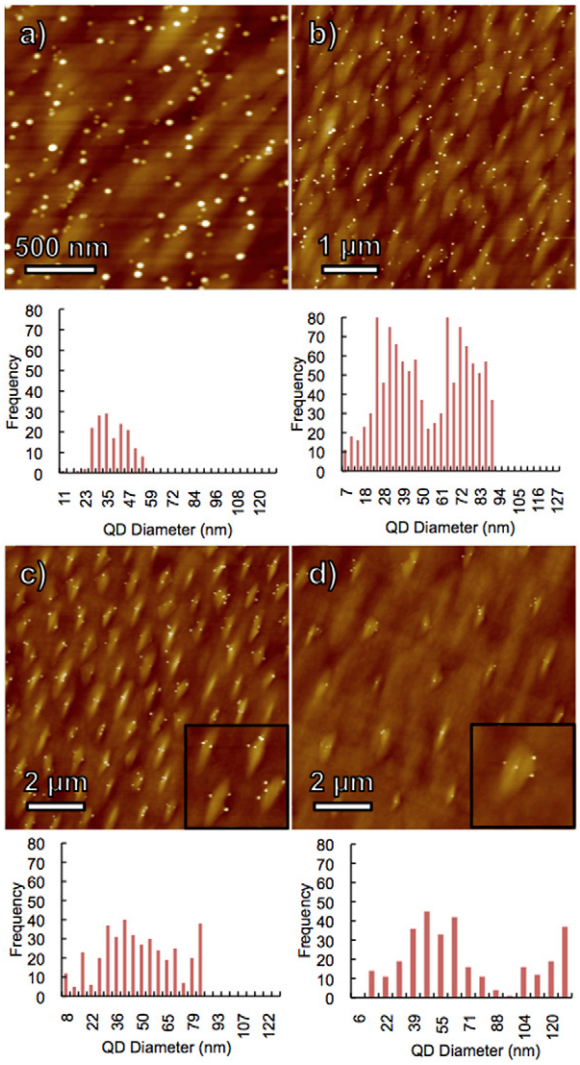

Figure 6. AFM images of the uncapped surface of the 26 layer sample for the 9.0 ms FIB dwell time patterns at pattern spacings of (a) 0.25 μm, (b) 0.5 μm, (c) 1.0 μm, and (d) 2.0 μm with a corresponding histogram of QD diameter distribution below each AFM image. The insets in (c) and (d) show higher magnification images of the mounds with QDs on them. The number of bins for each histogram was determined by the square root of the number of data points.

They attributed the mounds to the height of the underlying QDs, which was approximately half that of the spacer layer thickness [18, 21]. This was likely the case for the 26 layer sample as well, where the average QD height measured after six layers was 15 nm for the largest spacing and 5 nm for the smallest spacing at a 9.0 ms FIB dwell time. These QD heights are a large fraction of the spacer layer thickness, consistent with the hypothesis of Kiravittaya *et al*.

Although QDs formed on the mounds and retained the general periodicity of the original patterns for the 1.0 and 2.0 μm pattern spacings, the mounds are undesirable for several reasons. For closer pattern spacings, mound proximity destroyed the fidelity as seen in figures 6(a) and (b). Because the maximum lateral dimension of the mounds is $\sim$1 μm, the closest pattern spacing achievable without disrupting the

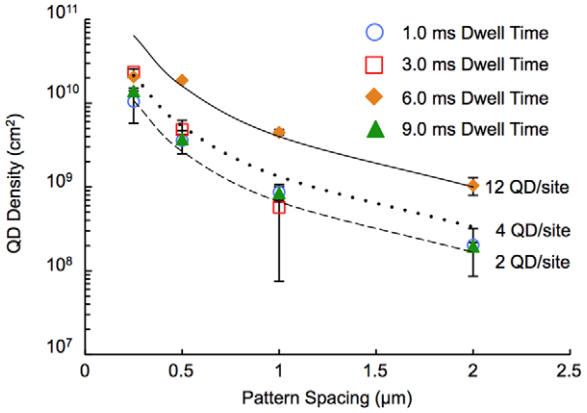

Figure 7. Plot of the QD density as a function of the pattern spacing as measured on the uncapped surface of the 26 layer sample for the 9.0 ms FIB dwell time. Error bars are not visible for all data points due to a small standard deviation for some of the measurements. The dashed and solid lines are explained in the text.

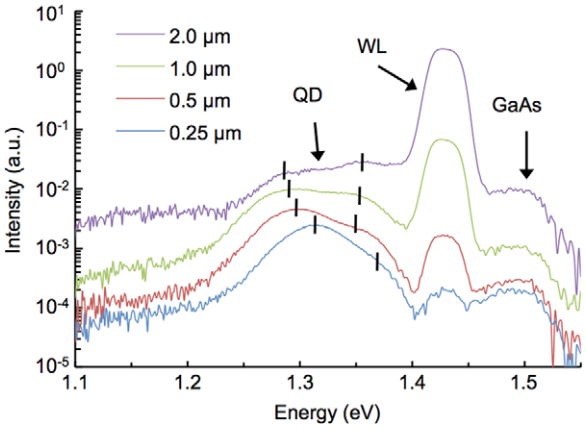

Figure 8. Photoluminescence spectrum from the 26 layer sample for the 9.0 ms FIB dwell time patterns showing the GaAs substrate peak at 1.49 eV, the wetting layer peak at 1.43 eV, and the QD peak between 1.27 and 1.35 eV. The split QD peak is a result of the bimodal QD distribution. The peak positions for the split QD peak are indicated by the tick marks. The measurements were taken at 15 K.

pattern is ∼0.7 μm when the pattern is oriented 45° off [1$\bar{1}$0]. Spacings as small as 0.3 μm can be achieved if the mounds are aligned along [1$\bar{1}$0] and allowed to overlap along that direction [18, 21]. However, control over QD position would suffer along the ridge forming from the overlapping mounds. In either case, mounds limit the highest achievable QD density and control over QD position. Interestingly, the QD density versus pattern spacing still followed the theoretical trend for QD density versus pattern spacing despite the loss of pattern fidelity. Figure 7 shows the QD density measured on the 26th layer as a function of pattern spacing and dwell time and dashed, dotted, and solid lines for theoretical densities assuming two, four, and 12 QDs per patterned site, respectively. As the FIB dwell time increased, the fidelity of mound formation above the underlying holes also increased. Because QDs tended to form only on the mounds and multiple dots formed per mound, the theoretical number of QDs per patterned site increased with increasing FIB dwell time. However, the 9.0 ms FIB dwell time corresponded to a theoretical density of two QDs/site instead of following the increasing trend. This is due to the larger length/width aspect ratio of the mounds for the 9.0 ms FIB dwell time, resulting in a lower step edge area per mound and a lower QD areal density for the 9.0 ms FIB dwell time pattern. Additionally, mound formation created multiple preferred nucleation sites for each FIB-patterned site, hindering control over QD density and position. Finally, a bimodal QD size distribution of the uncapped surface dots was measured via AFM. Histograms of the QD diameter distributions are shown in figure 6 for the 9.0 ms FIB dwell time patterns at each pattern spacing. The number of bins for each histogram was determined by the square root of the number of data points for the given pattern.

The bimodal size distribution was also evidenced by a split QD peak in the photoluminescence (PL) data. Figure 8 shows the PL spectra for the 9.0 ms FIB dwell time patterns at each pattern spacing. The sample was mounted in a helium flow cryostat at 15 K and pumped using a 633 nm helium–neon laser with 282.5 μW incident power focused through a 0.7 NA infinity corrected objective. The PL spectra were collected using a 0.75 m spectrometer with a 150 G mm^{-1} reflection grating and a single channel InGaAs detector. The GaAs substrate peak was at 1.49 eV, and the WL peak was at 1.43 eV. The QD peak, which split for spacings larger than 0.25 μm, was between 1.27 and 1.35 eV. The separation between the QD PL peaks increased with increasing pattern spacing, which corresponded to the increased separation of the average QD size as measured by AFM. Additionally, as the pattern spacing increased, the intensity of the QD peaks decreased while the WL peak intensity increased relative to the GaAs peak due to the lower QD density and larger WL area at larger pattern spacings [19].

4. Conclusions

In conclusion, we have demonstrated the ability to control QD position and size via *in vacuo* FIB patterning while varying the pattern spacing and hole size with up to 100% single QD per patterned site fidelity after six layers. The pattern spacing affects the QD dimensions, and measuring QD size with increasing pattern spacing provided an estimation of the maximum adatom diffusion length, which is determined by the particular growth conditions. Patterning also provided the ability to alter the WL thickness. Additionally, the size of the FIB-milled holes affects QD diameter and pattern fidelity. Mound formation upon increasing the total number of layers to 26 was detrimental to pattern fidelity, and created a bimodal QD size distribution for most larger pattern spacings as measured by AFM and evidenced by a split QD PL peak.

Acknowledgments

This material is based upon work supported as a part of the Center for Solar and Thermal Energy Conversion, an Energy

Frontier Research Center funded by the US Department of Energy, Office of Science, Office of Basic Energy Sciences under Award Number DE-SC0000957.

References

[1] Luque A and Marti A 1997 *Phys. Rev. Lett.* **78** 5014
[2] Marti A, Lopez N, Antolin E, Canovas E, Stanley C, Farmer C, Cuadra L and Luque A 2006 *Thin Solid Films* **511/512** 638–44
[3] Ledentsov N N *et al* 1996 *Phys. Rev.* B **54** 8743–50
[4] Bousaiene L, Ilahi B, Sfaxi L, Hassen F, Maaref H, Marty O and Dazord J 2004 *Appl. Phys.* A **79** 587–91
[5] Englund D, Fattal D, Waks E, Solomon G, Zhang B, Nakaoka T, Arakawa Y, Yamamoto Y and Vuckovic J 2005 *Phys. Rev. Lett.* **95** 013904
[6] Badolato A, Hennessy K, Atature M, Dreiser J, Hu E, Petroff P M and Imamoglu A 2005 *Science* **308** 1158
[7] McKay H, Rudzinski P, Dehne A and Millunchick J M 2007 *Nanotechnology* **18** 455303
[8] Atkinson P, Schmidt O G, Bremner S P and Ritchie D A 2008 *C. R. Physique* **9** 788–803
[9] Nakamura Y, Schmidt O G, Jin-Phillip N Y, Kiravittaya S, Muller C, Eberl K, Grabeldinger H and Schweizer H 2002 *J. Cryst. Growth* **242** 339–44
[10] Portavoce A, Hull R, Reuter M C and Ross F M 2007 *Phys. Rev.* B **76** 235301
[11] Hull R, Graham J F, Kubis A J, Portavoce A and Ross F M 2007 *Microsc. Microanal.* **13** (Suppl 2) 176–7
[12] Gherasimova M, Hull R, Reuter M C and Ross F M 2008 *Appl. Phys. Lett.* **93** 023106
[13] Lee J Y, Noordhoek M J, Smereka P, McKay H and Millunchick J M 2009 *Nanotechnology* **20** 285305
[14] Lee J, Saucer T W, Martin A J, Tien D, Millunchick J M and Sih V 2011 *Nano Lett.* **11** 1040–3
[15] Mehta M, Reuter D, Melnikov A, Wieck A D and Remhof A 2007 *Appl. Phys. Lett.* **91** 123108
[16] Mehta M, Reuter D, Melnikov A, Wieck A D and Remhof A 2008 *Physica* E **40** 2034–6
[17] Kiravittaya S, Benyoucef M, Zapf-Gottwick R, Rastelli A and Schmidt O G 2006 *Appl. Phys. Lett.* **89** 233102
[18] Kiravittaya S, Heidemeyer H and Schmidt O G 2004 *Physica* E **23** 253–9
[19] Saucer T W, Lee J, Martin A J, Tien D, Millunchick J M and Sih V 2011 *Solid State Commun.* **151** 269–71
[20] Cheng C C, Meneou K and Cheng K Y 2011 *J. Cryst. Growth* **323** 180–2
[21] Kiravittaya S, Rastelli A and Schmidt O G 2009 *Rev. Prog. Phys.* **72** 046502
[22] Xie Q, Madhukar A, Chen P and Kobayashi N P 1995 *Phys. Rev. Lett.* **75** 2542–5
[23] Howe P, Le Ru E C, Clarke E, Abbey B, Murray R and Jones T S 2004 *J. Appl. Phys.* **95** 6
[24] Gutierrez M, Herrera M, Gonzalez D and Garcia R 2006 *Appl. Phys. Lett.* **88** 193118
[25] Levchenko I and Ostrikov K 2009 *Appl. Phys. Lett.* **95** 243102
[26] Pimpinelli A and Einstein T L 2007 *Phys. Rev. Lett.* **99** 226102
[27] Wasilewski Z R, Fafard S and McCaffrey J P 1999 *J. Cryst. Growth* **201/202** 1131–5